JOURNAL OF SOLID STATE CHEMISTRY **128,** 121–129 (1997)
ARTICLE NO. SC967184

Metal-to-Metal Bonding in Transition Metal Monocarbides and Mononitrides

L'ubomír Benco

Institute of Inorganic Chemistry, Slovak Academy of Sciences, Dúbravská cesta 9, SK-84236 Bratislava, Slovak Republic

Received December 26, 1995; in revised form October 4, 1996; accepted October 10, 1996

The chemical bonding in transition metal carbides and nitrides is compared and contrasted *via* simplified interaction scheme. Different properties of *dd* bonding states are exemplified by VC and VN. Different patterns of the metal-to-metal bonding in these two compounds are investigated in terms of overlap populations. A modeling of (i) energy matching and (ii) orbital dimensions is performed to find out electronic reasons for dissimilarities in metal-to-metal bonding. The energy difference between interacting atomic levels is demonstrated as the reason for shift of the *pd* vs *dd* competition. In the nitride, the large value of ΔE_{pd} (2.4 eV) gives rise to the decreased *pd* bonding and increased net metal-to-metal bonding. The carbide having a small ΔE_{pd} (0.4 eV) displays the strengthened *pd* bonding, whereas net *dd* bonding practically vanishes. The larger overlap of atomic orbitals in the carbide results in the pronounced broadening of the *p* band toward higher binding energies. It does not influence, however, the net metal-to-metal bonding. © 1997 Academic Press

I. INTRODUCTION

The electronic structure of transition metal carbides and nitrides (TMCN) has been extensively studied during the past two decades, both experimentally and theoretically (Ref. (1) and references therein). These compounds show extreme values for properties such as melting point and hardness, which makes them interesting materials for technological applications (2). All of them show large deviations from stoichiometry having vacancies only in the nonmetal sublattice. The defect structure is an important property of these compounds since the vacancies are known to have a strong influence on the bulk properties such as superconductivity, specific heat, and paramagnetic susceptibility (2). Though several authors have discussed reasons for those defect structures (3), there seems to be no general agreement on this issue.

The stoichiometric TMCN, however, represents a starting point on our way toward an understanding of the properties of these materials. Their electronic structures are well understood (4). The valence region is dominated by the nonmetal *p* and transition metal (TM) *d* bands. Both carbides and nitrides exhibit an overlap of these bands, much larger in the former type of compounds. In carbides of transition metals of the fourth group (M^{IV}) of the Periodic Table, the Fermi level (E_F) is situated exactly inbetween these subbands. The valence region thus contains only a *d*-admixture to the *p* bands (5) and no real *d* bands appear in photoemission spectra (6). All carbides and nitrides of higher transition metals contain additional electrons accomodated in states of *d* bands. Photoemission spectra at different photon energies show increased intensity of these *d* bands with increased photon energy thus proving the *d* character of the bands situated just below E_F (1, 7). The results of numerous calculations (e.g., Ref. (4)) demonstrate an overall agreement between the calculated and experimental electronic structures of these compounds.

Recently, an analysis of the bonding properties of states in the valence region was reported for TMCN displaying the picture of the chemical bonding in the compact form of a crystal orbital (CO) scheme (8). When compared and contrasted for carbides and nitrides, the bonding shows differences in both the occupied and unoccupied energy region. Although discussions on the relative importance of the *p–d* and *d–d* bonding, supported by high precision X-ray diffraction, conclude that *d–d* bonding for TiC and TiN are similar (9), the recent analysis (8) has shown pronounced differences in the metal-to-metal bonding, demonstrating that a rigid band model is not valid for carbides and nitrides. In the nitride, the one extra electron per formula unit causes a shift of the Fermi level. This, however, cannot be the main reason for explaining the different properties of nitrides with respect to carbides. E.g., various first row TM carbides with the same rocksalt-type structure have rather similar properties (2) in spite of the fact that their respective Fermi levels vary within a large interval on the energy scale. The simple interaction scheme for TMCN (8) shows the separation of states into bonding, nonbonding, and antibonding ones. While bonding states provide for the overall stability of a particular compound, nonbonding states show

0022-4596/97 $25.00

negligible influence in this respect. The filling of antibonding states, however, results in a decreased stability. Extensive data collected by Toth (2) have demonstrated that carbides and nitrides of higher TM do not form stable stoichiometric phases. Searching for electronic reasons behind these distinct properties, one must focus on the bonding states. In the valence region these dominate up to the minimum in the density of states (DOS) between the *p* and the *d* bands. Although bonding states in carbides and nitrides come from both *pd* and *dd* interactions, the metal-to-metal bonding is much weaker than the *pd* bonding. Thus the interaction diagram is dominated by the stronger *pd* interactions (4, 5, 8) but cannot account for fine details. Therefore the origin for the differences in the metal-to-metal bonding needs a detailed analysis of those atomic features which determine the bonding.

This work presents electronic structure calculations on stoichiometric VC and VN (sodium chloride crystal structures (2)). The brief summary of their electronic structures, highlighting differences in the chemical bonding, is followed by detailed investigations of the metal-to-metal bonding in terms of overlap populations. Within the concept of atomic orbitals (AO), which are used to characterize the electronic structures, a model of atomic characteristics ((i) the energy separation between AOs and (ii) the size of AOs) is used to demonstrate the close relation between these atomic features and the bonding properties of valence states in stoichiometric VC and VN. This work should lead to a better understanding of the chemical bonding in simple cubic stoichiometric TMCN and thus provide the starting point for an investigation of more complex structures of this important class of compounds.

II. CHEMICAL BONDING IN VANADIUM CARBIDE AND VANADIUM NITRIDE

Differences in metal-to-metal bonding in carbides and nitrides are exemplified by vanadium carbide and vanadium nitride. Since band-structure calculations for the large group of carbides and nitrides, possessing the rocksalt-type structure, have been extensively reviewed (Ref. (4e)), we start with a brief summary of the overall electronic structures. Instead of the usual way of displaying chemical bonding in terms of energy bands, total and partial DOS, and electron density plots, CO schemes are reported. The CO scheme represents a simplified interaction diagram consisting of total DOS, atomic energy levels, and interaction lines. They indicate splitting of atomic states into bonding and antibonding counterparts. Figure 1 shows the CO schemes for stoichiometric VC and VN. The total DOS displayed within these schemes are obtained using the crystal orbital method (10a) of the EHT quality (10b) (parameters listed in Table 1). This methodology is approximate, not reliable quantitatively. It provides, however, a conceptual basis for understanding of electronic structures (18). The schemes in Fig. 1 show (in a compact form) the picture of orbital interactions leading to the final DOS distribution. Interaction lines demonstrate that two kinds of interatomic interactions control the distribution of valence states (orbital contributions in each band are documented in Fig. 2). The *pd* interaction of nearest neighbors is dominant (nonmetal-to-metal), supplemented with the metal-to-metal interaction (next nearest neighbors). Besides the similarity in the electronic structures

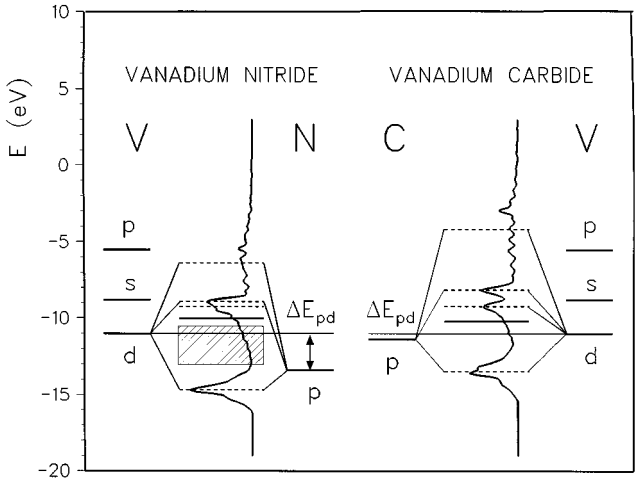

FIG. 1. The crystal orbital schemes for VC and VN. The DOS curve is assigned to a simplified interaction diagram showing a splitting of atomic levels into bonding and antibonding counterparts. The full horizontal line shows the position of the Fermi level within the DOS. Dashed lines indicate band positions. ΔE_{pd} highlights the energy difference between the interacting atomic levels. Interaction lines indicate the origin of states or bands leading to the total DOS. The lower main band consists of *pd* bonding states. The bands just above E_F consists of *dd* nonbonding and $pd(t_{2g})$ antibonding states (double line in VN, but two separated subbands in VC). The states forming the broad upper bands are due to the *p*-to-*d* (e_g) antibonding interaction (the center of mass of these bands is estimated according to the position of the e_g symmetry component).

TABLE 1
Orbital Parameters Used in Band Structure Calculations[a]

Atom	Orbital	H_{ii} (eV)	ζ_{i1}	(c_1)	ζ_{i2}	(c_2)
C	2*s*	− 21.4	1.625			
	2*p*	− 11.4	1.625			
N	2*s*	− 26.0	1.950			
	2*p*	− 13.4	1.950			
V	4*s*	− 8.81	1.300			
	4*p*	− 5.52	1.300			
	3*d*	− 11.0	4.750	0.4755	1.700	0.7052

[a] From "Table of Parameters for Extended Hückel Calculations," collected by Santiago Alvarez, Barcelona, 1985. H_{ii}, orbital ionization energies; ζ_{ij}, Slater exponents; c_j, coefficients in the double-zeta expansion of *d* orbitals.

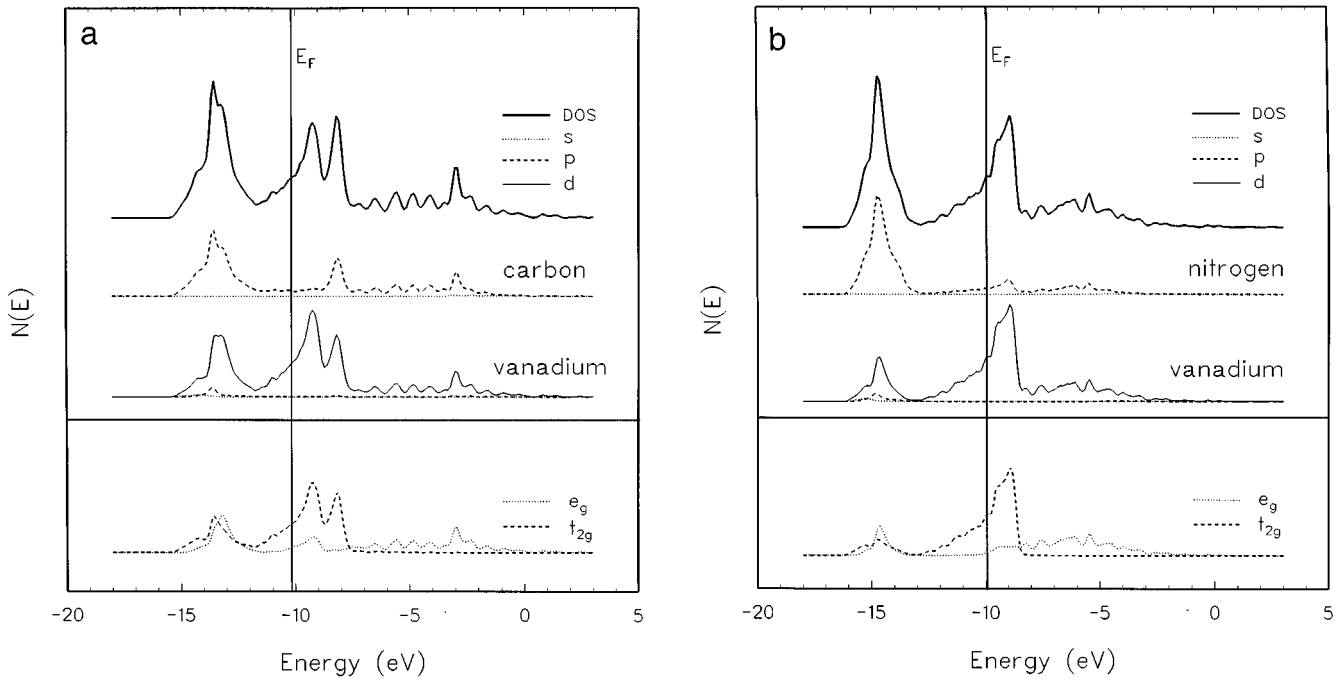

FIG. 2. Total and partial density of states: (a) vanadium carbide, (b) vanadium nitride. The number of states per energy interval (ordinate scale) is in arbitrary units, but kept the same for all curves. (a) and (b) demonstrate the dominant role of the nonmetal *p* and the metal *d* orbitals in the bonding of both compounds.

of VC and VN, differences are also apparent. The main features of the bonding are summarized as follows:

1. Nonmetal *p* and metal *d* orbitals dominate the chemical bonding (Fig. 2). *s* and *p* orbitals of the metal atom play a negligible role (Fig. 2). Therefore, in Fig. 1, no interaction lines for these levels are indicated.

2. The carbide is similar to a homonuclear system, since the energy difference between interacting nonmetal *p* and metal *d* levels is small ($\Delta E_{pd} = 0.4$ eV) in contrast to the nitride ($\Delta E_{pd} = 2.4$ eV).

3. The width of bands directly depends on the value of ΔE_{pd}. The smaller ΔE_{pd} leads to stronger covalent bonds, which are spread over a larger energy range thus giving rise to broader bandwidths. The width of the *p* bands is ≈ 4 and ≈ 3 eV for VC and VN, respectively. The stronger the covalent bonding the higher is the resistance of a material towards elastic deformation reflected in the bulk modulus. The bulk modulus of VC is 422 GPa (11). Though the value for VN is not available the bandwidth indicates that a value of ≈ 300 GPa could be estimated.

4. The valence region comprises three main bands. The *p* bands consists of both $pd(e_g)$ and $pd(t_{2g})$ bonding states (Fig. 2). The *d* bands just above E_F comprise *dd* nonbonding and $pd(t_{2g})$ antibonding states. The broad topmost bands (Figs. 1, 2) are due to the antibonding $pd(e_g)$ interaction. The bonding–antibonding splitting reflects the strength of an interaction. In VC and VN this splitting for the *p*-to-$d(t_{2g})$ interaction amounts to 4.7 and 3.4 eV (ΔE(bonding–antibonding) minus ΔE_{pd}). The corresponding melting points (2648 and 2177°C) and microhardnesses (28 and 15 GPa) (Ref. (2)) compare well with the trend in the bonding–antibonding splitting in stoichiometric compounds.

5. The band composition depends on ΔE_{pd}. In the carbide the small ΔE_{pd} causes that the *p* bands contain approximately 50% of both, C(2*p*) and V(3*d*) components (Fig. 2a and Refs. (13, 14)). In the nitride, the stabilizing bonding and/or the destabilizing antibonding shifts are smaller (Fig. 1). The bonding states are thus situated closer to atomic positions of the more electronegative atom. Consequently they are dominated by components coming from nitrogen atoms (N 2*p* states) (Fig. 2b and Refs. (13, 15)).

6. The metal-to-metal (*dd*) bonding is weaker than the metal-to-nonmetal (*pd*) bonding. The former gives rise neither to characteristic features, nor to fine structures in the DOS distribution (3, 8). DOS envelopes between the *p* and the *d* bands are similar displaying gradual increase toward the *d* bands. The states just below the Fermi level in VN, however, show bonding properties differing considerably from those in VC. The hatched area in the CO scheme (Fig. 1) highlights *d* states having different bonding properties. It shows the region of "net *dd* bonding states" which are not present in the carbide (8).

The detailed comparison of bandstructures of stoichiometric compounds with experimental data is difficult beacuse of everpresent defects on nonmetal lattice sites. Vacancies influence to some extent physical properties of compounds (some dependences are still not investigated, e.g., melting points vs vacancy concentration). The purpose of the comparison in points 3 and 4 above is to indicate the relation of physical quantities which are driven by the strength of the strongest (metal-to-nonmetal) bond and band structures in general. For carbides and nitrides these properties considerably differ due to the different degree of covalency/ionicity, which is well seen in their band-structures.

III. *pd* AND *dd* BONDING

The interaction scheme presented in Fig. 1 (cf. also (8)) shows that interactions of two kinds compete for the same set of *d* orbitals. The strong *pd* bonding is responsible for the characteristic features of the DOS distribution. The arrangement of atoms within the rocksalt-type structure allows also a metal-to-metal bonding, being much weaker than the metal-to-nonmetal one. This supplementary bonding, however, critically depends on the former main bonding. Any change in the *pd* bonding induces a modification of the *dd* interaction. E.g., strengthening of the *pd* interaction causes that a larger amount of *d* orbitals is involved in the *pd* interaction thus weakening the metal-to-metal interaction. Though the *pd* vs *dd* balance is substantially shifted towards the *pd* bonding, the weaker *dd* bonding also plays a role in TMCN. Carbides and nitrides are typical substoichiometric compounds. The question why nonstoichiometric phases are stable in a broad range of concentrations is still not answered. The nonstoichiometry is always due to vacancies in the nonmetal sublattice. When a nonmetal atom is missing the *pd* vs *dd* competition shifts toward strengthening of the metal-to-metal bonding. These bonds giving rise to bands of *dd* states below the Fermi level were also verified experimentally (1). As the rocksalt-type structure provides octahedral surrounding of the vacancy the *dd* bonding inside the void results in six-centered octahedral *dd* bonds (12). The *dd* bonding thus not only supports the creation of the nonstoichiometric phases, but octahedral bonds (OBs) show also pronounced directional properties. Recent investigation of OBs in TMCN (16) proves that the interaction of OBs is responsible for the formation of superstructures in substoichiometric TMCN. In carbides, this interaction leads to OBs stacked in the 111 plane while in long-range-ordered nitrides only corner shared octahedra occur (17). Two different kinds of superstructures in substoichiometric TMCN are clearly due to the different tendency of forming bonding states in stoichiometric carbides and nitrides.

An obvious procedure to investigate the bonding properties of states is the calculation of Mulliken overlap population for all states in a certain energy interval (18). It is positive (negative) for bonding (antibonding) states and approaches zero for nonbonding ones. The COOP quantity (crystal orbital overlap population) introduced by Hoffmann (18) are overlap population weighted DOS displaying bonding properties of states in a graphical form. Figure 3 shows the COOP curves for the *pd*, the *dd*, and the *pp* interaction. The thick full line indicates properties of valence states due to the interaction of nearest neighbors (*pd* interaction). The dotted line shows the metal-to-metal and the thin full line the nonmetal-to-nonmetal interaction of next nearest neighbors (*dd* and *pp* interaction). Note that the main differences in the bonding occur near the Fermi level.

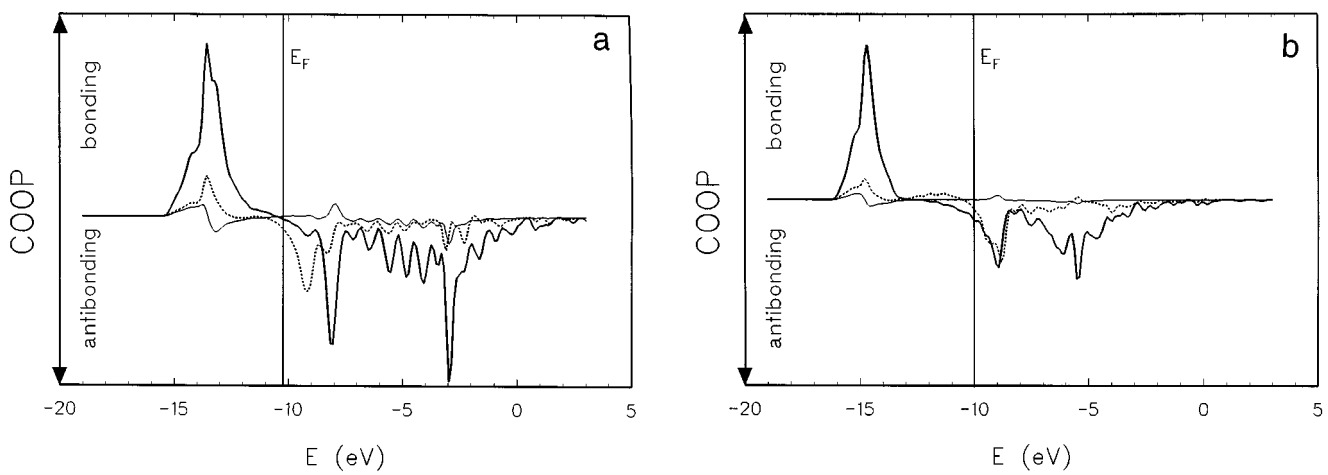

FIG. 3. Bonding properties of states displayed via the COOP curves for metal-to-nonmetal (full thick line), metal-to-metal (dashed line), and nonmetal-to-nonmetal (full thin line) interactions: (a) vanadium carbide; (b) vanadium nitride. The ordinate scale is in arbitrary units, but kept the same for all curves.

In the carbide states just below the E_F (Fig. 3a, energy range between ≈ -13 eV and E_F) diminishing *pd* bonding is shown, while the metal-to-metal interaction is nonbonding. The analysis of charge densities in the Γ point indicates also some $d(t_{2g})$–$d(t_{2g})$ bonding interaction falling into this energy interval. Extremely low weight of this high symmetry point, however, causes that the overall metal *d* densities appear nonbonding.

Figure 3a shows that states of the main bonding bands (situated at ≈ -14 eV) originate from three kinds of interaction. The *pd* interaction between nearest neighbors dominates. Much smaller contributions come from the bonding between next nearest neighbors. Carbon-to-carbon contacts provide both, bonding and antibonding states, the former situated at lower energies. *dd* bonding states appear also within these bands. Figure 4 shows a fragment of the rocksalt structure containing two metal and two nonmetal atoms. Bonding states of the *p* bands are due to the strong *pd* interaction (Fig. 4, right). Along with a σ overlap between *p* and *d* orbitals also a π overlap between *d* orbitals occurs (Fig. 4, right), therefore *pd* bonding states simultaneously show slight *dd* bonding. Figure 4 (left) illustrates an example of the orbital interaction where *p* orbitals cannot participate for symmetry reasons. This dd_π orbital interaction is much weaker than the *pd* one because of a larger interatomic distance and thus smaller AO overlap. States due to such interaction (net *dd* states) therefore should appear (if any) above the *p* bands. The broken line in Fig. 3a indicates that no such states are detected in the carbide.

The *d* bands situated above E_F split into two subbands (see the total DOS within the CO scheme in Fig. 1). Figure 3a shows the bonding characteristics of these states demonstrating clear *pd* nonbonding and *dd* antibonding character of states within the first subband (at ≈ -9.5 eV). On the other hand the second subband (≈ -8 eV) displays *pd* antibonding and rather *dd* nonbonding character of states. The reason why in carbide states of the *d* bands separate into two subbands could be the strong *pd* interaction (stronger than in VN). Figure 1 demonstrates the stabilizing/destabilizing shifts of energy levels due to the chemical bonding. The $pd(t_{2g})$ stabilization shifts (i.e., E_p(atomic)–E(*p* band) are 1.9 and 1.3 eV for the carbide and nitride, respectively. Similarly the destabilization of antibonding $pd(t_{2g})$ states in the carbide is higher (2.8 and 2 eV for VC and VN, respectively). This larger upward shift makes them well distinguished from the *pd* nonbonding states.

In the nitride (Fig. 3b), the dotted line indicates two regions of the metal-to-metal bonding interaction. States of main *p* bands (centred at ≈ -15 eV) are both *pd* and *dd* bonding (see Fig. 4, right, and the text above). The bonding *dd* states located between the *p* bands and the Fermi level (hatched area in Fig. 1) represent a new feature distinguishing nitride from carbide. Being spread over a large energy interval, these states display a *pd* nonbonding character. When approaching the Fermi level interactions of both kinds, *dd* and *pd*, turn antibonding. The main *d* bands situated ≈ 1 eV above the E_F (Fig. 1) show pronounced *dd* and also *pd* antibonding character of states. In analogy to the carbide, it could be anticipated that these bands comprise also *pd* nonbonding states. However, probably due to the weaker *pd* interaction (compared to carbide), most of the *d* states remain unaffected within the broad *d* bands.

IV. MODELING OF ATOMIC PARAMETERS

Within the concept of CO the bonding is determined by the overlap and an energy matching between atomic orbitals. The overlap depends on both, interatomic distances and the dimension of the AOs. Fortunately, the interatomic distances in VC and VN are similar ($r_{VC} = 2.09$ Å and $r_{VN} = 2.07$ Å). Moreover, preliminary results show that the slight change in the interatomic distance has a negligible effect on the electronic structure and bonding properties of the states under consideration (13). Therefore the analysis of fine features of bonding in VC and VN can be performed using the same interatomic distance $r_{VN} = 2.07$ Å. Differences in the *dd* bonding of carbide and nitride of the same transition metal, highlighted in the previous paragraph, are thus due to (i) ΔE_{pd} and (ii) different dimensions of nonmetal *p* orbitals. In the nitride, the *pd* vs *dd* competition is apparently shifted toward a weakened *pd* and strengthened *dd*

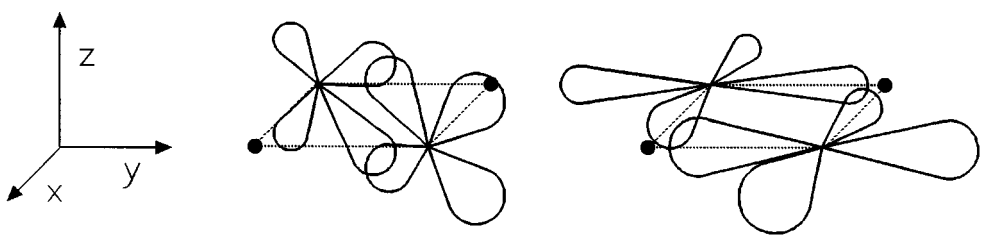

FIG. 4. An example of *dd* interactions in a rocksalt-type structure shows the net dd_π interaction (left) where nonmetal *p* orbitals cannot participate for symmetry reasons. *d* orbitals pointing toward nonmetal atoms (right) allow both, pd_σ and dd_π interactions. Full circles indicate positions of nonmetal atoms.

bonding. It is not clear, however, how each of these two factors influences the bonding, especially the metal-to-metal interaction.

ΔE Modeling

Figure 5 shows bonding properties of occupied *dd* states up to E_F. Metal-to-metal COOP curves for a series of parametrized electronic structure calculations of VN are displayed. The front curve characterizes the real vanadium nitride where the energy level of *p* orbitals (E_p) equals -13.4 eV (same as broken line in Fig. 3b). The next curves are obtained for $E_p s$ consecutively increased from the value of VN (-13.4 eV) to the value of VC (-11.4 eV; cf. Table 1). This simulation illustrates the effect of the energy separation on the metal-to-metal bonding keeping all other factors fixed (ΔE_{pd} ranges from 2.4 eV in VN to 0.4 eV in VC). The value of ΔE_{pd} determines both the relative intensities of the DOS bands and their positions. In the nitride ($E_p = -13.4$ eV), two groups of *dd* states exist: (i) states of the *p* bands centered at ≈ -15 eV and (ii) net *dd* states spreading approximately from -13 to -10.5 eV. The large energy difference between *p* and *d* levels results in a weakened *pd* bonding (compared to carbide); i.e., the number of *d* states situated within the *p* bands is decreased. Consequently the *pd* vs *dd* competition is shifted toward a strengthened *dd* bonding, giving rise to net *dd* bonding states situated at higher (less negative) energies. As ΔE_{pd} decreases (energy level of the nonmetal atom moves upward), *d* states become more involved in the *pd* bonding and the *dd* bonding diminishes. At $\Delta E_{pd} = 0.4$ eV, which is intrinsic to VC, the net *dd* bonding practically vanishes. Note that the *pd* bonding is not displayed in Fig. 4. Within the *p* bands, however, the *pd* and *dd* bonding are closely related (cf. Figs. 3a and 3b). As pointed out above, the *dd* bonding within the *p* bands is a byproduct of the *pd* bonding. Increased *dd* bonding therefore characterizes also the increased *pd* bonding. Figure 5 demonstrates the influence of ΔE_{pd} on the *pd* vs *dd* competition. The larger ΔE_{pd} supresses the *pd* bonding and supports the *dd* one (front curve) and vice versa. The maximized *dd* bonding interaction means that *d* orbital lobes point to each other (Fig. 4, left), while the *pd* bonds are maximized when *d* orbital lobes point to the ligand sites (Fig. 4, right). Thus the stronger the *pd* interaction, the more the *d* orbital lobes orient toward the *p* orbital lobes, thereby leading to a weakening of the *dd* interaction.

Positions of CO states depend on the position of the corresponding interacting atomic levels. Therefore the shift of the nonmetal *p* energy level induces also a shift of the bonding states. In Fig. 5, the positions of both bands move upwards with increased E_p. The shift of the atomic level by 2 eV, however, gives rise to a shift of the main bonding bands by only 1.6 eV (from -14.8 to -13.2 eV; Fig. 1). This could be explained by the increased bonding–antibonding splitting. Improved energy matching of interacting

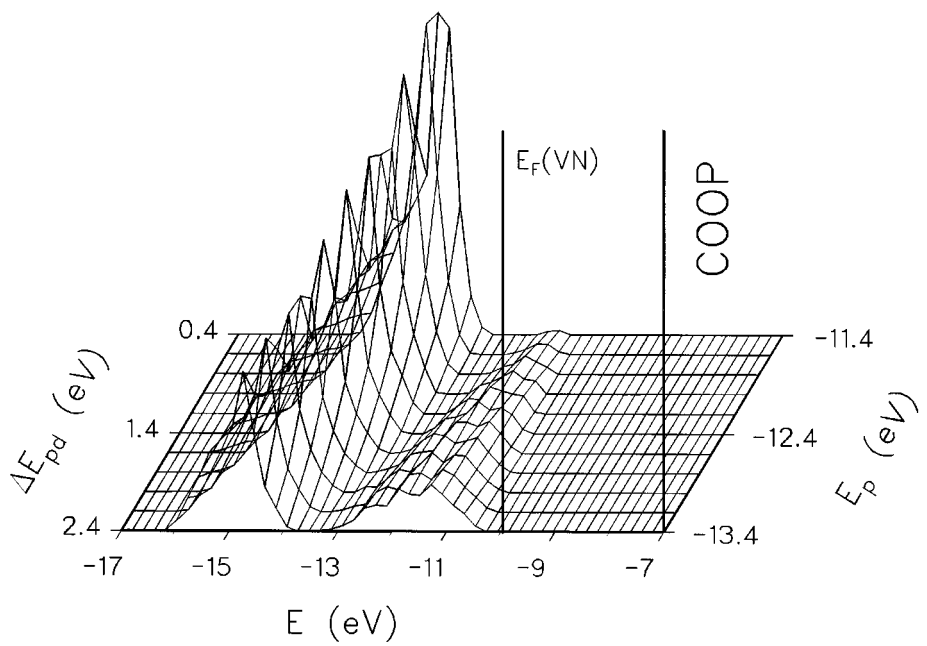

FIG. 5. The dependence of the metal-to-metal COOP curve on the energy separation between the interacting atomic levels. The left scale indicates the energy separation (ΔE_{pd}) and the right scale the energy level (E_p) of the nonmetal *p* functions. The front curve represents the COOP curve for vanadium nitride ($E_p = -13.4$ eV; $\Delta E_{pd} = 2.4$ eV). The vertical line indicates the Fermi level. Subsequent curves for increased $E_p s$ demonstrate the effect of improved energy matching ΔE_{pd} on the metal-to-metal bonding.

levels (going from nitride to carbide) causes a strengthening of the *pd* interaction, which results in a larger bonding–antibonding splitting. Thus states of the *p* bands in carbide become more stabilized and reside at deeper energies relatively to the E_p.

Modeling of Orbital Dimensions

A distribution of the electron density in bounded states (atoms, molecules, and solids) has been described above by means of AOs. The radial part of any AO characterizes the radial extent of the corresponding charge distribution. A useful simplified way of looking at the radial extent of orbitals is to speak about "orbital dimensions". Dimensions of *p* orbitals of carbon and nitrogen atoms differ due to their different electronegativity. The more electronegative nitrogen atom keeps its charge density distributed closer to its atomic nucleus than carbon. Therefore *p* orbitals of nitrogen are smaller than those of carbon which, on the contrary, are more diffuse. Increased dimensions of orbitals, however, raise the overlap between the metal *d* and the nonmetal *p* orbitals. As the overlap represents one of the main factors influencing the covalent bonding, modeling of orbital dimensions could shed light on relations between characteristic features of the bonding.

Figure 6 displays the dependence of the metal-to-metal bonding in vanadium nitride on the dimension of the nonmetal atom. The front curve in Fig. 6 represents the metal-to-metal COOP curve for VN. In the present computational procedure, the dimension of an orbital is adjusted by the Slater orbital exponent. Its value for the valence *p* orbital of the nitrogen atom is 1.950 (Table 1). The consecutive decrease of the exponent from 1.950 to 1.625 represents the expansion of *p* orbitals from nitrogen to carbon. Figure 6 demonstrates the effect of such an expansion on the metal-to-metal bonding. The two kinds of *dd* bonding in the nitride show only little effect. The net *dd* bonding ranging from ≈ -13 to ≈ -10.5 eV remains practically unchanged. The increased *pd* overlap raised by expanded *p* orbitals produces new *dd* states within the *p* bands centered at ≈ -15 eV. These states appear at the higher binding energy side, thus broadening the width of the main bonding bands from 3.2 (VN) to 4.5 eV. The investigation of orbital interactions between nearest neighbors, however, does not explain what is the origin of these states. Rather surprising is the finding that they correspond with the nonmetal-to-nonmetal bonding interaction. As already shown in Fig. 3, the *p* bands are strongly *pd* bonding, and comprise also the metal-to-metal and nonmetal-to-nonmetal bonding. The nonmetal-to-nonmetal interaction gives rise to states which are bonding, and also antibonding within the *p* bands. Most stabilized states, situated at the lower energy side of the *p* bands, are thus due to orbital interactions, which are bonding in all three kinds of interaction, *pd*, *dd*, and *pp*. Figure 7 illustrates the correspondence of the new states within the *p* bands and the nonmetal-to-nonmetal interaction. The front curve represents the nitrogen-to-nitrogen COOP curve for VN. The dependence shows that the

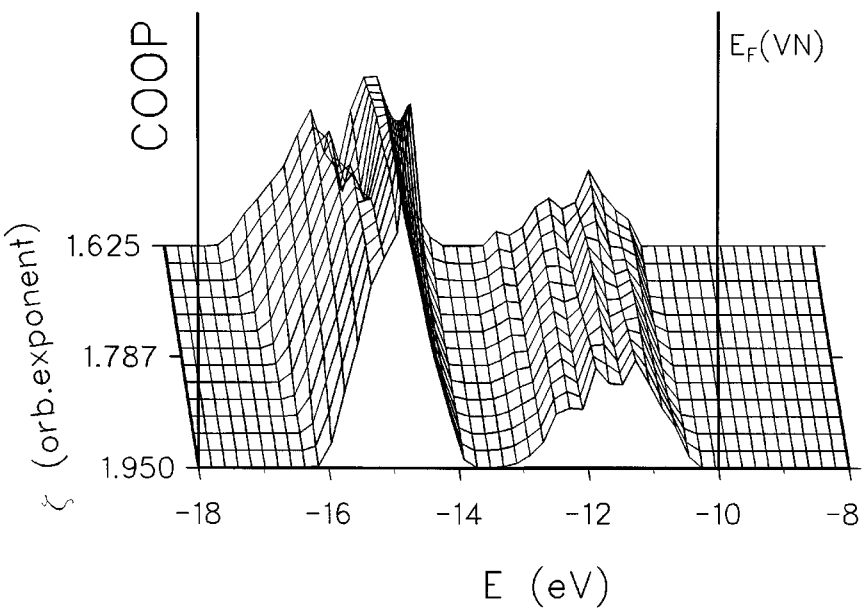

FIG. 6. The dependence of the metal-to-metal COOP curve on the dimension of the the nonmetal *p* orbital (characterized by an orbital exponent ζ). The front curve represents the true COOP curve for vanadium nitride. Subsequent curves show the effect of the expansion of the nonmetal *p* orbital (decreased ζ) on the metal-to-metal bonding. The rear curve ($\zeta = 1.625$) displays the distribution of *dd* states in a ficticious VN in which the nonmetal *p* orbitals are as large as those in a carbon atom.

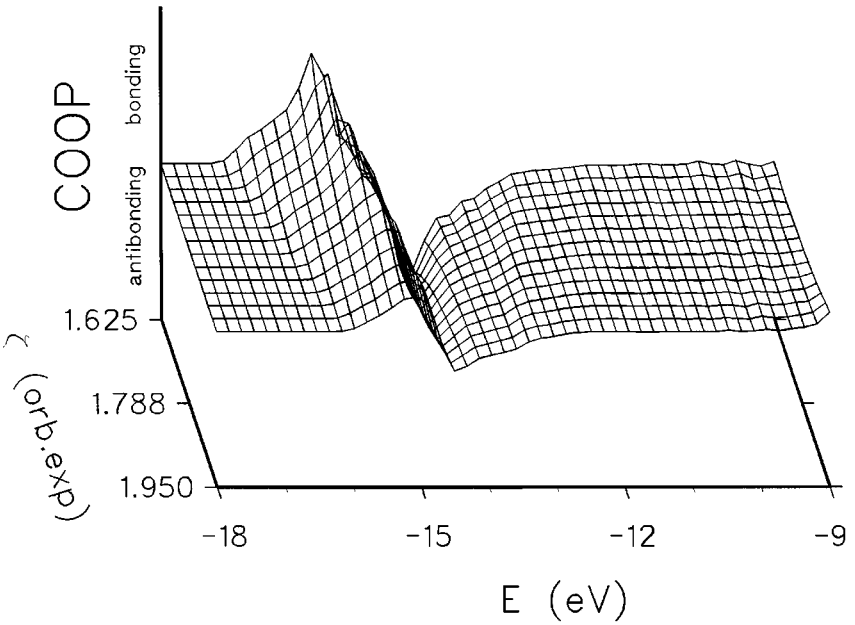

FIG. 7. The dependence of the nonmetal-to-nonmetal COOP curve on the dimension of the nonmetal *p* orbital. The front curve represents the true COOP curve for vanadium nitride. The expansion of orbitals causes the strengthening of the nonmetal-to-nonmetal bonding and also an increase of the bonding–antibonding splitting. The dependence shows the correspondence of new states in Fig. 6 and the nonmetal-to-nonmetal bonding states appearing due to the expansion of *p* orbitals.

increasing dimension of nonmetal *p* orbitals (from nitrogen to carbon) causes the strengthening of the nonmetal-to-nonmetal bonding. Note that the stronger is the interaction the larger is also the bonding–antibonding splitting. The bonding between second neighbors, however, is sensitive to interatomic distances. The shortening of the lattice constant toward nitride causes increased bonding between second neighbors. Therefore the nonmetal-to-nonmetal bonding in rocksalt TM carbides and nitrides is equally important (13). The combination of all three kinds of bonding interactions (*pd*, *dd*, and *pp*) gives rise to a shoulder (subband) located at the lower energy side of the *p* bands, clearly visible in DOS spectra of both carbides and nitrides.

V. CONCLUDING REMARKS

TMCNs with rocksalt-type structure allow a competition of two kinds of interaction (*pd* and *dd*) for the same set of *d* orbitals. The competition results in two different patterns of the metal-to-metal bonding inherent to carbides and nitrides. The present model calculations clearly indicate links between atomic features (ΔE_{pd} and dimension of the AO) and bonding properties of states in vanadium carbide and nitride. The *pd* vs *dd* competition is controlled by the value of ΔE_{pd}. In the nitride, the large ΔE_{pd} (2.4 eV) causes the weakened *pd* bonding and the strengthened net *dd* bonding. In the carbide ($\Delta E_{pd} = 0.4$ eV), the *pd* bonding dominates and the net *dd* bonding practically vanishes. The increased dimension of AOs of the nonmetal atom (larger pd_σ overlap) in VC does not influence the net *dd* bonding. It brings strengthening of the *pd*, *dd*, and *pp* interaction, thus giving rise to the pronounced broadening of the main bonding bands toward lower energies.

The present study demonstrates the important role of energy separation for chemical bonding. Unfortunately, this energy difference between the interacting atomic levels has not been reported in older papers on electronic structures. An interpretation of the chemical bonding in solids is often supported by various kinds of interaction diagrams (4e, 18, 19). All of them, however, use energy levels in a schematic form without an energy scale. The crystal orbital scheme introduced recently (8) uses total DOS positioned on the energy scale completed with relevant atomic levels and interaction lines. This interaction diagram assigns the main features of the DOS curve showing the atomic origin of states within all bands. True positions of atomic levels highlight the energy matching which not only determines the shape of the total DOS, but provides also an insight into the covalency/ionicity of the bonding (larger ΔE gives rise to more ionic bonds). From the present analysis, it is clear that the value of ΔE can account for rather fine effects like a competition for *d* orbitals in *pd* vs *dd* interactions. The conclusions of the present work emphasize the usefulness of presenting the bonding in solids in the form of crystal orbital schemes.

The interaction schemes presented for VC and VN are valid for monocarbides and mononitrides of the whole first row transition metals having the rocksalt-type structure.

The bonding mechanism in titanium carbide and nitride was shown to obey similar relations to those for vanadium compounds (8). The main difference is that the *pd* vs *dd* balance is more pronounced. The *pd* bonding in TiC is stronger than that in VC because of the larger pd_σ overlap. In TiN the *dd* bonding becomes stronger (compared to VN) due to the larger ΔE_{pd} (2.6 eV). Since the value of ΔE_{pd} for all first row TMCN ranges from 0 to 2.6 eV, a similar relation between the *pd* and *dd* bonding occurs for the whole group of compounds as that demonstrated in Fig. 4. An increased number of electrons, however, causes the Fermi level to shift upward. Due to the fact that there are no further bonding states (all additional states are either nonbonding or antibonding from both *pd* and *dd* interactions), all stoichiometric carbides and nitrides of higher TMs are energeticallly unfavourable. Starting with chromium, the carbides and nitrides prefer formation of substoichiometric compounds or derived structures (2). All of these defect-stabilized compounds show increased metal-to-metal bonding (compared to the stoichiometric counterparts). The mechanism giving rise to multicentered bonds indicates that states identified as net *dd* states in stoichiometric compounds become components of multicentered bonds within vacancies (12). Stronger net *dd* bonding (caused by larger ΔE_{pd}) in stoichiometric compounds results in stronger multicentered bonds induced by the creation of a vacancy. The finding that the *pd* vs *dd* competition is controlled by the value of ΔE_{pd} holds also for defect-stabilized compounds. Recent total energy ab initio calculations performed on ordered structures of $VC_{0.75}$ and $VN_{0.75}$ (16) demonstrate that stronger multicentered bonds provide stronger interactions raised by neighboring vacancies in the structure. This was demonstrated for substoichiometric rocksalt-type structures (16). Other structures of the first row TMCN allowing multicentered metal-to-metal bonds are supposed to obey similar relations between the *pd* and *dd* bonding.

ACKNOWLEDGMENTS

This work was supported in part by the Slovak Grant Agency VEGA (Grant No. 1172). The author is grateful to R. Hoffmann for his comments and encouragement. S. Reschke is thanked for useful disscussions, and reviewers of the manuscript are acknowledged for many helpful suggestions.

REFERENCES

1. L. I. Johansson, *Surf. Sci. Rep.* **21,** 177 (1995).
2. L. Toth, "Transition Metal Carbides and Nitrides." Academic Press, London, 1971.
3. (a) V. P. Zhukov, N. I. Medvedeva, and V. A. Gubanov, *Phys. Status Solidi B* **151,** 407 (1989); (b) B. M. Klein, D. A. Papaconstantopoulos, and L. L. Boyer, *Phys. Rev. B* **22,** 1946 (1980); (c) L. M. Huisman, A. E. Carlsson, C. D. Gelatt, Jr., and H. Ehrenreich, *Phys. Rev. B* **22,** 991 (1980).
4. (a) A. Neckel, K. Schwarz, R. Eibler, P. Weinberger, and P. Rastl, *Ber. Bunsenges. Phys. Chem.* **79,** 1053 (1975); (b) P. Blaha and K. Schwarz, *Int. J. Quantum Chem.* **23,** 1535 (1983); (c) J. Redinger, R. Eibler, P. Herzig, A. Neckel, R. Podloucky, and E. Wimmer, *J. Phys. Chem. Solids* **47,** 387 (1986); (d) W. E. Pickett, B. M. Klein, and R. Zeller, *Phys. Rev. B* **34,** 2517 (1986); (e) K. Schwarz, *CRC Crit. Rev. Solid State Mater. Sci.* **13,** 211 (1987).
5. (a) A. Neckel, P. Rastl, R. Eibler, P. Weinberger, and K. Schwarz, *J. Phys. C* **9,** 579 (1976); (b) P. Marksteiner, P. Weinberger, A. Neckel, R. Zeller, and P. H. Dederichs, *Phys. Rev. B* **33,** 6709 (1986).
6. (a) J. H. Weaver, A. M. Bradshaw, J. F. van der Veen, F. J. Himpsel, D. E. Eastman, and C. Politis, *Phys. Rev. B* **22,** 4921 (1980); (b) A. M. Bradshaw, J. F. van der Veen, F. J. Himpsel, and D. E. Eastman, *Solid State Commun.* **37,** 37 (1980); (c) C. G. Larsson, J. B. Pendry, and L. I. Johansson, *Surf. Sci.* **162,** 19 (1985); (d) K. L. Håkansson, L. I. Johansson, P. L. Wincott, and D. S. L. Law, *Surf. Sci.* **251/252,** 108 (1991).
7. S. V. Didziulis, J. R. Lince, T. B. Stewart, and E. A. Eklund, *Inorg. Chem.* **33,** 1979 (1994).
8. L'. Benco, *Solid State Commun.* **94,** 861 (1995).
9. A. Dunand, H. D. Flack, and K. Yvon, *Phys. Rev. B* **31,** 2299 (1985).
10. (a) J. M. Andre, *J. Chem. Phys.* **50,** 1536 (1969); (b) M. H. Whangbo, M. Evain, T. Hungbanks, M. Kertesz, S. D. Wijeyesekera, C. Wilker, C. Zheng, and R. Hoffmann, QCPE Program No. 571, Indiana Univ., 1988.
11. T. B. Shaffer, *in* "Engineered Materials Handbook" (S. J. Schneider Tech. Chairman), Ceramics and Glasses, Vol. 4, p. 804. ASM International, Materials Park, OH, 1991.
12. L'. Benco, *J. Solid State Chem.* **110,** 58 (1994).
13. L'. Benco, unpublished results.
14. P. Marksteiner, P. Weinberger, A. Neckel, R. Zeller, and P. H. Dederichs, *Phys. Rev. B* **33,** 812 (1986).
15. P. Blaha and K. Schwarz, *Phys. Rev. B* **36,** 1420 (1987).
16. L'. Benco, *J. Solid State Chem.* **111,** 440 (1994).
17. (a) C. H. de Novion and V. Maurice, *J. Phys. Colloq.* **38**(C7), 211 (1977); (b) B. V. Khaenko, *Neorg. Mater.* **15,** 1535 (1979); (c) C. H. de Novion and J. P. Landesman, *Pure Appl. Chem.* **57,** 1391 (1985).
18. (a) S. D. Wijeyesekera and R. Hoffmann, *Organometallics* **3,** 949 (1984); (b) R. Hoffmann, "Solids and Surfaces: A Chemist's View of Bonding in Extended Structures." VCH, New York, 1988.
19. (a) J. Silvestre and R. Hoffmann, *Langmuir* **1,** 621 (1985); (b) Y. T. Wong and R. Hoffmann, *J. Chem. Phys.* **95,** 859 (1991); (c) E. Ruiz, S. Alvarez, R. Hoffmann, and J. Bernstein, *J. Am. Chem. Soc.* **116,** 8207 (1994).